Title

Oxygen Vacancies of Anatase(101): Extreme Sensitivity to the Density Functional Theory Method

Journal

Journal of Chemical Theory and Computation, 12(6)

ISSN

1549-9618

Authors

Haa, Mai-Anh
Alexandrova, Anastassia N

Publication Date

2016-06-14

DOI

10.1021/acs.jctc.6b00095

Peer reviewed

JCTC Journal of Chemical Theory and Computation

Article

pubs.acs.org/JCTC

Oxygen Vacancies of Anatase(101): Extreme Sensitivity to the Density Functional Theory Method

Mai-Anh Ha[a†] and Anastassia N. Alexandrova*[,†,‡]

[†]Department of Chemistry & Biochemistry, University of California, Los Angeles, California 90095, United States

[‡]California NanoSystems Institute, Los Angeles, California 90095, United States

ABSTRACT: We present a systematic investigation of the influence of theoretical parameters on the characterization of surface and subsurface oxygen vacancies in anatase with the 101 facet exposed. This metastable phase of titania continues to resist a facile description of its defects, particularly, in the reduced state. Nine nonequivalent sites were examined under varying levels of theory with characterization of formation energies, geometry, and electronic states extracted from Bader charges, charge density, and density of states. At DFT+*U* levels of theory, these sites remain nonequivalent. We note a new surface oxygen vacancy minimum related to localization of electrons at surface and a subsurface Ti atoms, rather than the more favorable localization at neighboring surface Ti atoms.

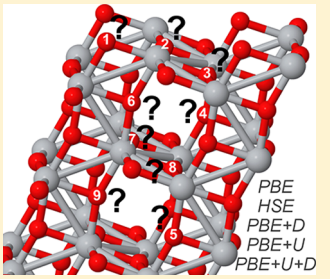

1. INTRODUCTION

The anatase surface remains ubiquitous in the field of catalysis for its unique photoactivity,[1−3] tunable through the use of dopants,[4,5] or size and structural selection,[6−8] and reactivity, such as water-splitting[9,10] and the decomposition of organic pollutants.[11,12] Both theory and experiment have cited surface defects such as oxygen vacancies to be a major contributing factor in anatase's catalytic activity. Although recent theoretical studies have concentrated on the more reactive 001 facet,[13] a return to the more thermodynamically stable 101 facet[14] reveals interesting subtleties, regarding the presence of surface and subsurface oxygen vacancies.

Previous studies neglected spin polarization and used semilocal functional Perdew−Burke−Ernzerhof (PBE)[15] in collaboration with scanning tunneling microscopy (STM) studies[16,17]to establish the formation of subsurface oxygen vacancies to be favored over that of surface vacancies. However, a recent STM study found that surface oxygen vacancies formed in the presence of a high positive sample bias or an electric field.[18] Under experimental conditions, such as an electrochemical cell, the presence of a potential bias and electric field would guarantee the formation of surface oxygen vacancies. Anatase remains a complex system to understand, both experimentally and computationally. This study will strive to elucidate a complete computational description of oxygen vacancies in anatase (101) under varying parameters available to density functional theory (DFT).

While the use of a semilocal functional may correct, in some part, the tendency in DFT calculations to overdelocalize electrons, it still falls short in reflecting the moderate to extreme localization present in semiconductors and insulators.[19] Strongly correlated systems that feature localized d- or f-orbitals require a hybrid functional or a DFT+*U* (LDA+*U* or GGA+*U*) approach to reflect the properties of this system in agreement with experiments. This becomes especially important in nonstoichiometric systems, such as those containing oxygen vacancies. When a neutral oxygen vacancy is present, the additional two electrons from this defect may localize on nearby Ti atoms, reducing Ti^{4+} to Ti^{3+}.[20,21] Moreover, spin-restricted and generalized gradient approximation (GGA) calculations neglect the magnetic properties of oxygen-deficient TiO_2.[22] Previous theoretical studies using a hybrid functional or a DFT+*U* approach recovered the antiferromagnetism of reduced anatase,[23] a band gap of >3 eV typical of TiO_2 (PBE underestimates at 1.77 eV),[24] and gap states ∼1 eV below the conduction band found in the experiment.[22,25] These studies have primarily focused on characterizing the effects of an oxygen vacancy in bulk anatase.

Although the DFT+*U* formalism describes the oxygen vacancy in the rutile phase of TiO_2 well, both in the bulk and on the surface, the results for anatase remain ambiguous. Bulk anatase featured quasi-degenerate simple and split geometries, i.e., the two electrons from a neutral oxygen vacancy either localized on a single Ti atom together or individually localized on neighboring Ti atoms.[20] Allen et al.'s occupation matrix control, which investigated specific occupation of d- and f-orbitals, found the same localization as DFT+*U* and identified the stability of integer occupation of d_{-2}-, d_{-1}-, and d_1-orbitals.[21] Moreover, the incorporation of nonlocal effects such as dispersion forces using Grimme's method[26] (the DFT+D formalism) correctly predicted the thermodynamic stability of the phases of TiO_2 (rutile > brookite > anatase).[27]

Clarification of the presence of surface and subsurface oxygen vacancies with additional computational parameters such as those mentioned above has not been pursued. This study proposes a comprehensive 3-fold approach in accounting for the presence of surface and subsurface oxygen vacancies (V_O). These parameters include spin polarization, localization of the two electrons due to V_O, through the Hubbard *U*-value, and

Received: January 28, 2016

DOI: 10.1021/acs.jctc.6b00095
J. Chem. Theory Comput. XXXX, XXX, XXX−XXX

consideration of long-range interactions such as London dispersion and van der Waal forces. These parameters will be investigated individually and in combination, in order to explore the method dependence of the formation of oxygen vacancies in anatase. Results will be compared to the experiment. Finazzi et al. had explored the dependence of U in bulk anatase, specifying a U range of 3−4 eV to best reflect experimental data, and that range will be pursued here for surface anatase.[22]

2. COMPUTATIONAL METHODOLOGIES

All plane wave density functional theory (PW-DFT) calculations were performed with the QUANTUM ESPRESSO package.[28−31] Spin-restricted and unrestricted calculations were performed employing the PBE[15] functional and using the most recently available ultrasoft pseudo-potentials[32] with scalar relativistic corrections. The PBE functional was used in all cases. For brevity, DFT+PBE+D is referred to as DFT+D and DFT+PBE+U, DFT+U. All calculations were spin-unrestricted, except for the system labeled "Spin Restricted" in Tables 1 and 2 (given later in this work), in order to recover the presence of localized electrons forming Ti^{3+} states. The gap states caused by these Ti^{3+} states will be further discussed in the following section. Large kinetic energy cutoffs of 32 (320) Ry were applied to the wave functions (charge density). For comparison, calculations utilizing the screened hybrid functional by Heyd, Scuseria, and Ernzerhof (HSE) were also pursued.[33,34] The implementation of HSE required use of norm-conserving pseudo-potentials with the PBE potential and kinetic energy cutoffs of 32 (128) Ry, with respect to the wave functions (charge density).[35] The HSE functional with 25% Hartree−Fock (HF) exchange and a screening parameter of ω = 0.200 $bohr^{-1}$ was able to reproduce anatase's band gap (see Table 1).[36] Janotti et al.'s values of 20% HF exchange and ω = 0.106 $bohr^{-1}$ (~0.200 $Å^{-1}$) were also tested. For their study, these parameters yielded accurate band gaps and lattice constants for the rutile phase of TiO_2. However, for our anatase slab, these same parameters resulted in large band gaps of >3.60 eV and are not further reported here. All calculations were done at the Γ point with a convergence threshold of 10^{-6} Ry implemented during SCF cycles.

The anatase slab was modeled with lattice constants of a = 3.7845 Å, c = 9.5143 Å from experimental crystallographic data.[37] The appropriate cuts were made to construct the most stable and dominant facet (>94%) of the anatase crystal, the 101 surface, as a cell of 16 TiO_2 units.[14] This cell was first relaxed in the bulk under a Monkhorst−Pack grid of 4 × 4 × 4 centered at Γ and then doubled along the z-axis for a total of 96 atoms. In surface calculations, the bottom third was fixed to reflect the bulk and ~12 Å vacuum gap was added to minimize spurious effects between periodic cells. In order to facilitate calculations and post-processing, lattice vectors that describe an orthorhombic cell were used. Post-processing of calculations was done with QUANTUM ESPRESSO to generate charge density files and projected density of states (PDOS) plots. Visualization of charge density difference was generated through VESTA.[38] The Bader charge algorithm for PW-DFT was used to analyze shifts in electron density, following the formation of an oxygen vacancy.[39]

Note that, for ease of comparison, the surfaces utilized in this study were grown from a bulk unit cell modeled from experimental crystallographic data. Other sample cases were examined under a denser k-point mesh (DFT+D+(U = 3.6) with 3 × 3 × 1) or with an optimized lattice constant (DFT+(U = 3.6)). Both of these cases resulted in some changes to the energy, but did not change resulting trends in the lowest three to four minima of oxygen vacancies as listed in Tables 1 and 2 (presented later in this work). These conditions resulted in a minimum whose geometry was midway between the initial and final geometries described in Figure 2. This is not surprising, given the sensitivity of oxygen vacancy sites to computational parameters (as evidenced below in Figures 2 and 3 and the following section, Results and Discussion).

3. RESULTS AND DISCUSSION

The formation energies of oxygen vacancies were calculated using the equation below:

$$E_{form}(V_O) = E_{tot}(\text{def}) - E_{tot}(\text{no def}) + \frac{1}{2}\mu(O_2)$$

where E_{tot}(def) represents the total energy of defective anatase, E_{tot}(no def) represents the total energy of stoichiometric anatase, and $\mu(O_2)$ is the total energy of an O_2 molecule. The reference energies of stoichiometric anatase and oxygen were calculated under the same conditions as the defective anatase. Figure 1 illustrates the cell and possible oxygen vacancy sites,

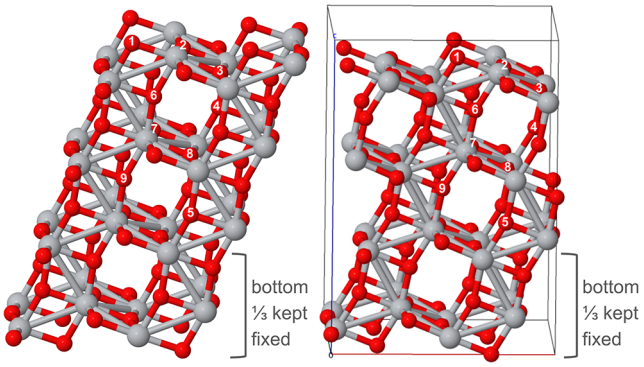

Figure 1. Depiction of a 32 TiO_2 unit cell with oxygen vacancies (V_O) labeled. (Left) A monoclinic cell is displayed for ease of viewing the nonequivalent sites for oxygen vacancy formation. (Right) For calculations and post-processing, the lattice vectors were modified to represent an orthorhombic cell (a = 9.869 Å, b = 7.569 Å, c > 25 Å, α = β = γ = 90°).

V_{O1-O9}, and Table 1 lists the lowest formation energies. The trend in formation energies at other sites, as compared to the minimum, is presented in Table 2. Cheng et al. had previously investigated sites V_{O1-O6} under DFT+PBE, and V_{O1} and V_{O4} under DFT+U.[16,40] Slight differences in formation energies are a result of our more rigorous kinetic energy cutoff and cell size. Although Cheng et al. found V_{O5} to be particularly stable at larger cell sizes of 216 atoms, we did not find this to occur in our cell. The formation energy of V_{O5} remained >0.5 eV from the minimum.

Because of the interest in anatase for photocatalysis and solar cell use, the band gaps (E_g) of stoichiometric and reduced anatase were extracted from PDOS plots (see Table 1 for energies, Figure 5 (presented later in this work) for plots). Projected density of states (PDOS) plots will be discussed in conjunction with surface oxygen vacancy formation. Typically, DFT underestimates the band gaps of materials with DFT+U, providing some correction to increase the band gap, and hybrid functions or GW many-body perturbations, providing the best

DOI: 10.1021/acs.jctc.6b00095
J. Chem. Theory Comput. XXXX, XXX, XXX−XXX

Table 1. Lowest Formation Energy (E_{Form}) and Band Gaps (E_g) of Oxygen Vacancy under Varying Computational Parameters[a]

system	V_O	vacancy site	settings	E_{Form} (eV)	$E_{g,stoich}$ (eV)	$E_{g,def}$ (eV)
I	9	subsurface (see Figure 3)	spin-restricted	3.88	1.72	1.67
II	9	subsurface (see Figure 3)	spin-polarized	3.88	1.71	1.62, 1.71
III	1	surface	DFT+D	4.19	1.72	1.58
IV	1	surface	DFT+(U = 3.0)	4.12	2.02	2.10
V	1	surface	DFT+(U = 3.6)	3.82	2.10	2.15
VI	1	surface	DFT+(U = 4.0)	3.61	2.15	2.22
VII	1	surface	DFT+D+(U = 3.6)	3.93	2.10	2.15
VIII	1	surface	HSE ($HF_{0.25}$, $PBE_{0.75}$)	2.91	3.21	3.20
			experiment		3.2,[b] 3.4[c]	

[a]Note: Band gaps (E_g) were calculated from density of states (DOS) plots of both stoichiometric (stoic) and defective (def) anatase with the lowest oxygen vacancy formation energy. There are two values for spin-polarized calculations on the defective surface, because of the splitting at the conduction band. The total DOS plots revealed a shift in energy apart of the spin-up and spin-down components at the conduction band resulting in two different band gaps. Systems II–VIII are spin-unrestricted. [b]Data taken from refs 42 and 43. [c]Data taken from ref 44.

Table 2. Sorted Formation Energy (ΔE_F), with Respect to Minimum of Oxygen Vacancy under Varying Computational Parameters[a]

I		II		III		IV		V		VI		VII		VIII	
Spin-Restricted (DFT+PBE)		Spin-Polarized (DFT+PBE)		DFT+D		DFT+(U = 3.0)		DFT+(U = 3.6)		DFT+(U = 4.0)		DFT+D+ (U = 3.6)		HSE ($HF_{0.25}$, $PBE_{0.75}$)	
V_O	ΔE_F (eV)	V_O	ΔE_F (eV)	V_O	ΔE_F (eV)	V_O	ΔE_F (eV)	V_O	ΔE_F (eV)	V_O	ΔE_F (eV)	V_O	ΔE_F (eV)	V_O	ΔE_F (eV)
9	0.00	9	0.00	1	0.00	1	0.00	1	0.00	1	0.00	1	0.00	1	0.00
4	0.05	4	0.05	9	0.00	6	0.35	6	0.31	9	0.78	6	0.32	4	0.39
6	0.22	6	0.22	6	0.01	4	0.49	4	0.73	5	0.78	4	0.83	6	0.50
1	0.23	1	0.23	4	0.02	5	0.68	3	0.92	8	0.81	3	0.93	5	0.83
5	0.85	5	0.70	5	0.58	9	0.70	5	0.92	6	0.82	5	0.98	7	0.89
8	0.93	8	0.90	8	0.74	8	0.80	9	0.93	7	0.84	9	0.98	9	0.89
7	1.05	7	0.98	7	0.81	7	0.82	8	0.99	4	0.89	8	1.02	8	0.90
3	1.30	3	1.23	3	1.01	3	0.86	7	1.02	3	1.01	7	1.04	3	1.21
2	1.83	2	1.70	2	1.49	2	1.32	2	1.38	2	1.10	2	1.40	2	1.22

[a]Note: In all systems except for System I, spin-restricted (DFT+PBE) calculations were spin-polarized and often exhibited gap states of localized Ti^{3+} in projected density of states (PDOS) plots.

correction to directly reproduce the experiment.[22,24,41] Since the band gap is a bulk property, the band gaps calculated for surfaces will not necessarily be reflective of the bulk. He et al. observed that the anatase surface is particularly sensitive to experimental conditions, displaying color changes from orange-clear to darker blue, so band gaps extracted from surface calculations might still be of considerable interest.[17] Our values of the band gap at the surface are not unusual for DFT with E_g ≈ 1.7 eV and DFT+U with E_g ≈ 2.1. HSE reflected the most accurate band gap with E_g ≈ 3.2 eV for both stoichiometric and defective anatase. In our calculations, DFT+D resulted in a slight decrease in the band gap, but the effect was negligible in conjunction with Hubbard U. The presence of an oxygen vacancy produces a slight compression of the band gap under DFT+PBE and DFT+D and slight expansion under DFT+U and DFT+D+U levels of theory.

In our systematic investigation of oxygen vacancy formation in anatase, we found a significant dependence on computational parameters in influencing not only the geometry and energy of surface and subsurface sites V_{O1} and V_{O4}, but also many other sites. Notably, further analysis of V_{O6} and V_{O9} yielded other unique, DFT-method-dependent minima (see Figure 2 and 4 (presented later in this work) on V_{O6}, Figure 3 on V_{O9}). Cheng et al. noted that subsurface site V_{O6} is unstable, resulting in the surface O_{2c} filling the site (in Figure 2, surface O_{2c} are colored green, for the sake of clarity). Our investigations show that this

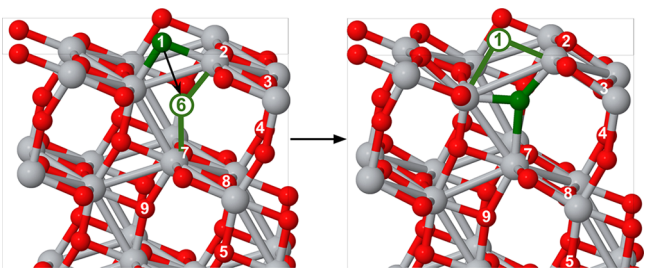

Figure 2. Under the DFT+D, DFT+(U = 3.0, 3.6), and DFT+D+(U = 3.6) formalism, the surface oxygen O_{2c} (colored green) will migrate to fill the vacancy site V_{O6} during geometric relaxation. This results in a surface oxygen vacancy, whose electronic structure is identical to the one formed through vacancy site V_{O1} under DFT+D, but remains unique, compared to V_{O1} under the DFT+U and DFT+D+U (see Figure 4).

occurs in all calculations except for DFT+(U = 4.0) and HSE, whether we remain at the DFT+PBE level or continue in complexity toward the DFT+D, DFT+(U = 3.0, 3.6), and DFT+D+(U = 3.6) formalism.

In comparison to V_{O6}, the formation of V_{O9} remains unstable only at DFT+PBE and DFT+D levels of theory and minimizes to form a distorted V_{O4} (see Figure 3). This phenomenon at sites V_{O6} and V_{O9} reinforces the need for acknowledgment and understanding of the theoretical parameters in use to

DOI: 10.1021/acs.jctc.6b00095
J. Chem. Theory Comput. XXXX, XXX, XXX–XXX

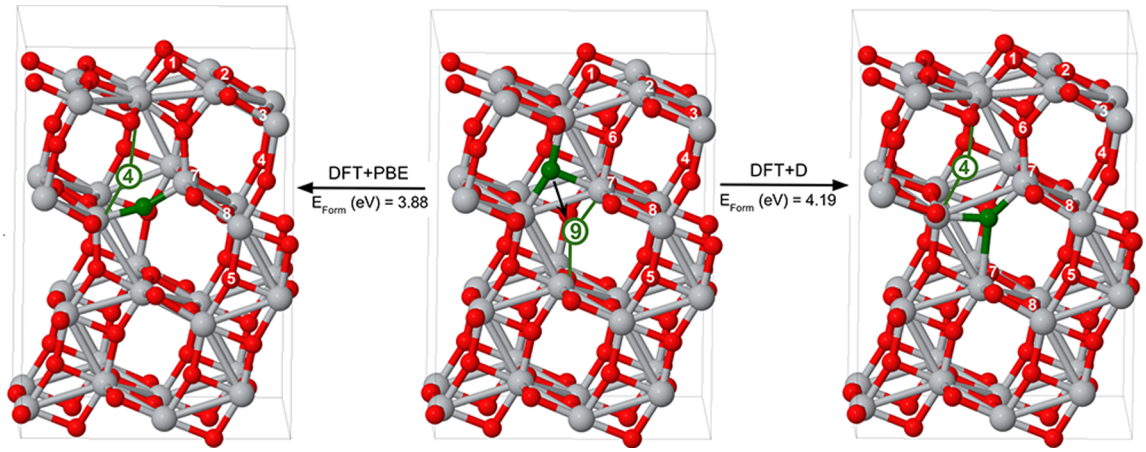

Figure 3. Creation of an oxygen vacancy V_{O9} (green, labeled) is unstable in DFT+PBE and DFT+D calculations, resulting in the oxygen above (green) attempting to fill the site (indicated by a black arrow). The resulting geometry is that of a distorted subsurface oxygen vacancy with the site symmetry of V_{O4} (green, labeled). These are the global minima of DFT+PBE and DFT+D calculations.

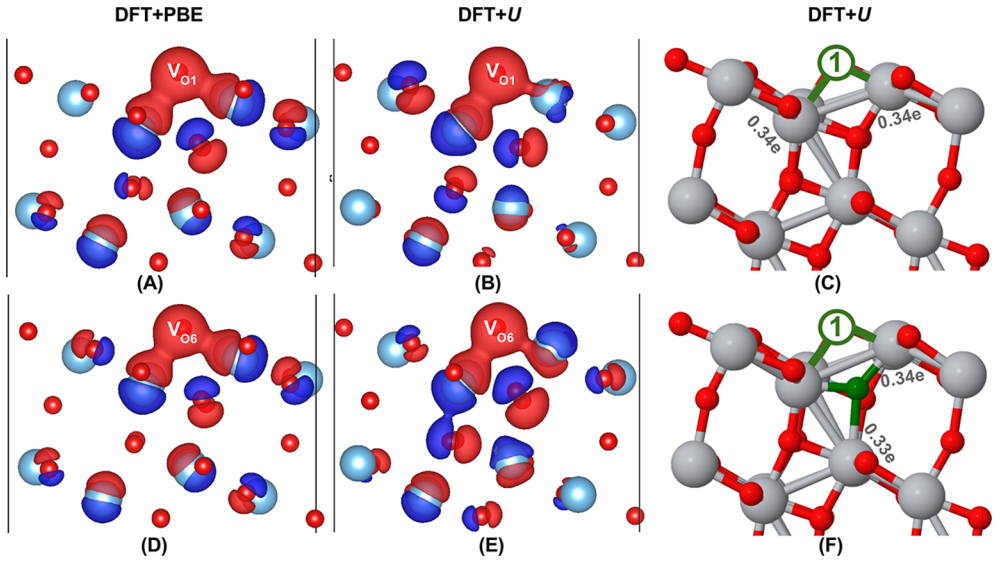

Figure 4. Isosurfaces of defective anatase depicting the difference in charge density, with respect to the stoichiometric cell. The considered defects are the surface oxygen vacancy resulting from V_{O1} (top) and surface oxygen vacancy resulting from V_{O6} (bottom, see Figure 2 for labels). Red represents a negative difference in charge density and blue denotes a positive difference, with respect to the stoichiometric cell. Surface oxygen vacancy formed from minimization of site V_{O1} or site V_{O6} is indicated on the image. (A, D) In the DFT+PBE and DFT+D formalism, the differences in charge density remain negligible between the surface oxygen vacancy formed by minimization of V_{O1} and V_{O6}. (B, E) In the DFT+U and DFT+D +U formalism, the surface oxygen vacancy formed by V_{O6} results in more extreme shifts in the electron density of atoms surrounding the site. (C, F) Under the DFT+(U = 3.6), Bader charges at neighboring Ti atoms for a surface oxygen vacancy formed from site V_{O1} (C, electronic occupations at surface Ti) and from site V_{O6} (F, electronic occupations at surface and subsurface Ti).

characterize oxygen vacancies in anatase. At DFT+PBE and DFT+D levels of theory, V_{O1} and V_{O6} (see Figure 2 for formation of the surface oxygen vacancy), V_{O4} and V_{O9} (see Figure 3 for formation of the subsurface oxygen vacancy) are almost interchangeable, resulting in the same minimum. At DFT+(U = 4.0) and HSE, all V_O sites remain stable. Moreover, the formation energies of these sites reflect the symmetry of their coordination to other atoms. The energies become increasingly degenerate for vacancies formed deeper in the cell; V_{O7} and V_{O8} are almost degenerate, while sites V_{O5} and V_{O9} are degenerate.

Under the DFT+U formalism, the surface oxygen vacancy that results from minimization of V_{O6} differs from surface oxygen vacancy V_{O1}. Plots of the difference in charge density, with respect to the stoichiometric cell, reveal subtle shifts in the electron density at the subsurface oxygen vacancy cite (see Figure 4). Bader charge analysis pinpoints the shift. Integration of the density along the zero flux surface results in occupation of ∼0.3−0.4 e on neighboring titanium atoms. The localization of electrons on two Ti atoms differs between the resulting surface oxygen vacancy from V_{O4} and V_{O1}. At V_{O1}, a localization of ∼0.3−0.4 e occurs on both surface Ti atoms that are connected to V_{O1}, while the localization is split between the surface Ti and subsurface Ti atom bridged by V_{O6}. A shift of ∼0.3−0.4 e is significant, with respect to the original charge of +2.2 e on Ti atoms, reflective of the mixed ionic−covalent nature of the Ti−O bonds in semiconductor titania, characteristic of easily reducible oxides.[45] The subsurface oxygen vacancy V_{O6} is stable only at the DFT+(U = 4.0) and HSE levels of theory, but atoms are significantly distorted around the site,

DOI: 10.1021/acs.jctc.6b00095
J. Chem. Theory Comput. XXXX, XXX, XXX−XXX

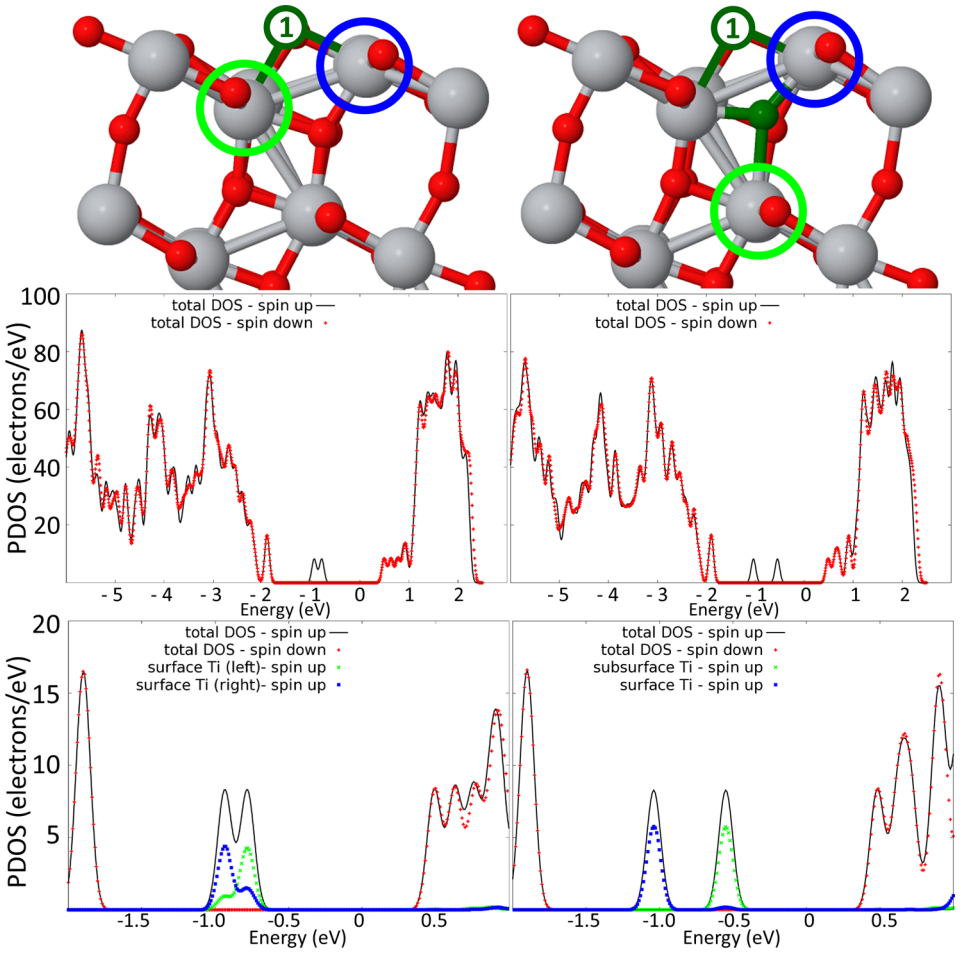

Figure 5. (Left) Density of states (DOS) plots depicting localization of electrons in the band gap on surface Ti atoms with the formation of a surface oxygen vacancy at V_{O1}. (Right) DOS plots of electrons localized on the surface and subsurface Ti atoms with the formation of a surface oxygen vacancy from V_{O6} (for visualization of this process, see Figure 2). The top graph displays the total DOS, with respect to spin, and the bottom graph illustrates features of the partial DOS of Ti's *d*-orbitals. Energies are shifted with respect to the Fermi energy set at zero. These plots are from DFT+D+(U = 3.6) calculations.

resulting in a higher formation energy. Surprisingly, the shift in electronic occupation between the DFT+(U = 4.0) and HSE is different. In DFT+(U = 4.0), the occupation resembles that of a surface oxygen vacancy, localizing at the Ti atoms below V_{O1}, whereas, with HSE, the occupation remains at the neighboring Ti atoms, 0.45 e at the surface Ti and 0.46 e at the subsurface Ti.

The two surface oxygen vacancies are further examined through PDOS plots (Figure 5), which show band-gap states comparable to experiment, displaying Ti^{3+} states ~1 eV below the conduction band.[46,47] Moreover, the PDOS of *d*-orbitals of neighboring Ti atoms corroborates features observed in charge density difference plots and Bader charge analysis. The characterization of the formation of a surface oxygen vacancy from site 1 and site 6 by PDOS reinforces their unique identity. An oxygen vacancy formed at V_{O1} presents close, overlapping peaks in the band gap states related to the neighboring surface Ti atoms. Smearing occurs due to the similarity between the neighboring surface Ti atoms, both feature 4 Ti−O bonds. In contrast, a surface oxygen vacancy resulting from V_{O6} presents distinct split peaks ~0.5 eV from each other as a resulting of the differing coordination of the Ti atoms: surface Ti coordinates to 4 O atoms and subsurface Ti to 6 O atoms. In other words, this electron experiences an electrostatic penalty by localizing in the bulk, as opposed to the surface resulting in the $\Delta E_{form} \approx 0.3$ eV.

The geometries of these surface oxygen vacancies may be comparable, but their electronic occupations are not and may influence future studies on the catalysis and binding of small molecules.[48,49] Furthermore, in a recent STM study, the formation of surface oxygen vacancies was observed to be a result of subsurface oxygen vacancy clusters migrating to the surface.[18] Setvin et al. suggested that the presence of a positive potential bias or electric field from the STM tip led to the injection of "hot" electrons into the surface that aided in the migration of subsurface vacancies to the surface. These migrations resulted in pair and triangular formations of surface oxygen vacancies, which may have been stabilized and precipitated by these unequal occupations on neighboring Ti atoms.

4. CONCLUSIONS

In this theoretical study on oxygen vacancies, we have shown the influence of computational parameters on the energy, geometry, and electronic occupation of these vacancies. While there have been many studies conducted for bulk anatase or surface anatase with an oxygen vacancy at V_{O1} or V_{O4}, none have attempted a comprehensive outlook on all nonequivalent

DOI: 10.1021/acs.jctc.6b00095
J. Chem. Theory Comput. XXXX, XXX, XXX−XXX

sites and their subsequent optimization beyond PBE. Under the DFT+U formalism, analysis of these nonequivalent sites resulted in the discovery of two distinct surface oxygen vacancies related to their component reduced Ti^{3+} states. This may affect future studies regarding catalysis of small molecules on surface anatase or aggregation of clusters of oxygen vacancies. This study is meant to inform and guide future modeling of defective anatase(101) to be aware of the dependence of results on computational parameters on oxygen vacancies.

Since the formation of surface versus subsurface oxygen vacancies in anatase(101) seems to be condition-dependent in experiment as well as in theory, the choice of DFT method lies in what material properties are currently being investigated. DFT studies comparing to experiments under ultrahigh vacuum might neglect dispersion and Hubbard U corrections to preferentially treat subsurface oxygen vacancies while those considering catalysis in the presence of a potential gradient (as in photocatalysis related to electrochemical cells) may well include dispersion and Hubbard U corrections or hybrid levels of theory to consider surface oxygen vacancies. Moreover, consideration of gap states in experimental DOS absolutely requires spin-unrestricted, Hubbard U or hybrid levels of theory.

AUTHOR INFORMATION

Corresponding Author

*E-mail: ana@chem.ucla.edu.

Author Contributions

The manuscript was written through contributions of all authors. All authors have given approval to the final version of the manuscript.

Notes

The authors declare no competing financial interest.

ACKNOWLEDGMENTS

This work was supported by the Air Force Office of Scientific Research (No. BRI 10029173-S3), and NSF Career Award (No. CHE1351968). Computational resources were provided by the UCLA-IDRE cluster and the Air Force Research Laboratory's Spirit cluster.

REFERENCES

(1) Henderson, M. A. A surface science perspective on photocatalysis. *Surf. Sci. Rep.* **2011**, *66*, 185−297.

(2) Fujishima, A.; Zhang, X.; Tryk, D. A. TiO_2 photocatalysis and related surface phenomena. *Surf. Sci. Rep.* **2008**, *63*, 515−582.

(3) Linsebigler, A. L.; Lu, G.; Yates, J. T., Jr. Photocatalysis on TiO_2 surfaces: Principles, mechanisms, and selected results. *Chem. Rev.* **1995**, *95*, 735−758.

(4) Batzill, M.; Morales, E. H.; Diebold, U. Influence of nitrogen doping on the defect formation and surface properties of TiO_2 rutile and anatase. *Phys. Rev. Lett.* **2006**, *96*, 026103.

(5) Pham, H. H.; Wang, L. Electronic structures and current conductivities of B, C, N and F defects in amorphous titanium dioxide. *Phys. Chem. Chem. Phys.* **2015**, *17*, 11908−11913.

(6) Luttrell, T.; Halpegamage, S.; Tao, J.; Kramer, A.; Sutter, E.; Batzill, M. Why is anatase a better photocatalyst than rutile?—Model studies on epitaxial TiO_2 films. *Sci. Rep.* **2014**, *4*, 4043 DOI: 10.1038/srep04043.

(7) Close, T.; Tulsyan, G.; Diaz, C. A.; Weinstein, S. J.; Richter, C. Reversible oxygen scavenging at room temperature using electrochemically reduced titanium oxide nanotubes. *Nat. Nanotechnol.* **2015**, *10*, 418−422.

(8) Yang, H. G.; Sun, C. H.; Qiao, S. Z.; Zou, J.; Liu, G.; Smith, S. C.; Cheng, H. M.; Lu, G. Q. Anatase TiO_2 single crystals with a large percentage of reactive facets. *Nature* **2008**, *453*, 638−641.

(9) Tilocca, A.; Selloni, A. Reaction pathway and free energy barrier for defect-induced water dissociation on the (101) surface of TiO_2-anatase. *J. Chem. Phys.* **2003**, *119*, 7445−7450.

(10) Tilocca, A.; Selloni, A. Structure and reactivity of water layers on defect-free and defective anatase TiO_2 (101) surfaces. *J. Phys. Chem. B* **2004**, *108*, 4743−4751.

(11) Zhao, W.; Ma, W.; Chen, C.; Zhao, J.; Shuai, Z. Efficient degradation of toxic organic pollutants with $Ni_2O_3/TiO_{2-x}B_x$ under visible irradiation. *J. Am. Chem. Soc.* **2004**, *126*, 4782−4783.

(12) Wang, C.; Groenzin, H.; Shultz, M. J. Comparative study of acetic acid, methanol, and water adsorbed on anatase TiO_2 probed by sum frequency generation spectroscopy. *J. Am. Chem. Soc.* **2005**, *127*, 9736−9744.

(13) Selloni, A. Crystal growth: Anatase shows its reactive side. *Nat. Mater.* **2008**, *7*, 613−615.

(14) Lazzeri, M.; Vittadini, A.; Selloni, A. Structure and energetics of stoichiometric TiO_2 anatase surfaces. *Phys. Rev. B: Condens. Matter Mater. Phys.* **2001**, *63*, 155409.

(15) Perdew, J. P.; Burke, K.; Ernzerhof, M. Generalized gradient approximation made simple. *Phys. Rev. Lett.* **1996**, *77*, 3865.

(16) Cheng, H.; Selloni, A. Surface and subsurface oxygen vacancies in anatase TiO_2 and differences with rutile. *Phys. Rev. B: Condens. Matter Mater. Phys.* **2009**, *79*, 092101.

(17) He, Y.; Dulub, O.; Cheng, H.; Selloni, A.; Diebold, U. Evidence for the predominance of subsurface defects on reduced anatase TiO_2 (101). *Phys. Rev. Lett.* **2009**, *102*, 106105.

(18) Setvin, M.; Schmid, M.; Diebold, U. Aggregation and electronically induced migration of oxygen vacancies in TiO_2 anatase. *Phys. Rev. B: Condens. Matter Mater. Phys.* **2015**, *91*, 195403.

(19) Himmetoglu, B.; Floris, A.; de Gironcoli, S.; Cococcioni, M. Hubbard-corrected DFT energy functionals: The LDA U description of correlated systems. *Int. J. Quantum Chem.* **2014**, *114*, 14−49.

(20) Morgan, B. J.; Watson, G. W. Intrinsic n-type defect formation in TiO_2: A comparison of rutile and anatase from GGA U calculations. *J. Phys. Chem. C* **2010**, *114*, 2321−2328.

(21) Allen, J. P.; Watson, G. W. Occupation matrix control of d- and f-electron localisations using DFT U. *Phys. Chem. Chem. Phys.* **2014**, *16*, 21016−21031.

(22) Finazzi, E.; Di Valentin, C.; Pacchioni, G.; Selloni, A. Excess electron states in reduced bulk anatase TiO_2: comparison of standard GGA, GGA+U, and hybrid DFT calculations. *J. Chem. Phys.* **2008**, *129*, 154113.

(23) Yang, K.; Dai, Y.; Huang, B.; Feng, Y. P. Density-functional characterization of antiferromagnetism in oxygen-deficient anatase and rutile TiO_2. *Phys. Rev. B: Condens. Matter Mater. Phys.* **2010**, *81*, 033202.

(24) Janotti, A.; Varley, J.; Rinke, P.; Umezawa, N.; Kresse, G.; Van de Walle, C. Hybrid functional studies of the oxygen vacancy in TiO_2. *Phys. Rev. B: Condens. Matter Mater. Phys.* **2010**, *81*, 085212.

(25) Sanjines, R.; Tang, H.; Berger, H.; Gozzo, F.; Margaritondo, G.; Levy, F. Electronic structure of anatase TiO_2 oxide. *J. Appl. Phys.* **1994**, *75*, 2945−2951.

(26) Grimme, S.; Antony, J.; Ehrlich, S.; Krieg, H. A consistent and accurate *ab initio* parametrization of density functional dispersion correction (DFT-D) for the 94 elements H-Pu. *J. Chem. Phys.* **2010**, *132*, 154104.

(27) Conesa, J. C. The relevance of dispersion interactions for the stability of oxide phases. *J. Phys. Chem. C* **2010**, *114*, 22718−22726.

(28) Giannozzi, P.; Baroni, S.; Bonini, N.; Calandra, M.; Car, R.; Cavazzoni, C.; Ceresoli, D.; Chiarotti, G. L.; Cococcioni, M.; Dabo, I.; et al. QUANTUM ESPRESSO: A modular and open-source software project for quantum simulations of materials. *J. Phys.: Condens. Matter* **2009**, *21*, 395502.

(29) Kohn, W.; Sham, L. J. Self-consistent equations including exchange and correlation effects. *Phys. Rev.* **1965**, *140*, A1133.

DOI: 10.1021/acs.jctc.6b00095
J. Chem. Theory Comput. XXXX, XXX, XXX−XXX

(30) Lee, C.; Yang, W.; Parr, R. G. Development of the Colle–Salvetti correlation-energy formula into a functional of the electron density. *Phys. Rev. B: Condens. Matter Mater. Phys.* **1988**, *37*, 785.
(31) Burke, K.; Werschnik, J.; Gross, E. Time-dependent density functional theory: Past, present, and future. *J. Chem. Phys.* **2005**, *123*, 062206.
(32) Vanderbilt, D. Soft self-consistent pseudopotentials in a generalized eigenvalue formalism. *Phys. Rev. B: Condens. Matter Mater. Phys.* **1990**, *41*, 7892.
(33) Heyd, J.; Scuseria, G. E.; Ernzerhof, M. Hybrid functionals based on a screened Coulomb potential. *J. Chem. Phys.* **2003**, *118*, 8207–8215.
(34) Heyd, J.; Scuseria, G. E.; Ernzerhof, M. Erratum: "Hybrid functionals based on a screened Coulomb potential" [*J. Chem. Phys.* 118, 8207 (2003)]. *J. Chem. Phys.* **2006**, *124*, 219906.
(35) Troullier, N.; Martins, J. L. Efficient pseudopotentials for plane-wave calculations. *Phys. Rev. B: Condens. Matter Mater. Phys.* **1991**, *43*, 1993.
(36) Krukau, A. V.; Vydrov, O. A.; Izmaylov, A. F.; Scuseria, G. E. Influence of the exchange screening parameter on the performance of screened hybrid functionals. *J. Chem. Phys.* **2006**, *125*, 224106.
(37) Howard, C.; Sabine, T.; Dickson, F. Structural and thermal parameters for rutile and anatase. *Acta Crystallogr., Sect. B: Struct. Sci.* **1991**, *47*, 462–468.
(38) Momma, K.; Izumi, F. VESTA 3 for three-dimensional visualization of crystal, volumetric and morphology data. *J. Appl. Crystallogr.* **2011**, *44*, 1272–1276.
(39) Tang, W.; Sanville, E.; Henkelman, G. A grid-based Bader analysis algorithm without lattice bias. *J. Phys.: Condens. Matter* **2009**, *21*, 084204.
(40) Cheng, H.; Selloni, A. Energetics and diffusion of intrinsic surface and subsurface defects on anatase TiO_2 (101). *J. Chem. Phys.* **2009**, *131*, 054703.
(41) Patrick, C. E.; Giustino, F. GW quasiparticle bandgaps of anatase TiO_2 starting from DFT U. *J. Phys.: Condens. Matter* **2012**, *24*, 202201.
(42) Tang, H.; Berger, H.; Schmid, P.; Levy, F.; Burri, G. Photoluminescence in TiO_2 anatase single crystals. *Solid State Commun.* **1993**, *87*, 847–850.
(43) Tang, H.; Berger, H.; Schmid, P. E.; Lévy, F. Optical properties of anatase (TiO_2). *Solid State Commun.* **1994**, *92*, 267–271.
(44) Tang, H.; Levy, F.; Berger, H.; Schmid, P. Urbach tail of anatase TiO_2. *Phys. Rev. B: Condens. Matter Mater. Phys.* **1995**, *52*, 7771.
(45) *Defects at Oxide Surfaces*; Jupille, J., Thornton, G., Eds.; Springer Series in Surface Sciences, No. *58*; Springer: Heidelberg, Germany, 2015 (ISBN 978-3-319-14367-5).
(46) Jackmana, M. J.; Deák, P.; Syres, K. L.; Adell, J.; Thiagarajan, B.; Levy, A.; Thomas, A. G. Observation of vacancy-related polaron states at the surface of anatase and rutile TiO_2 by high-resolution photoelectron spectroscopy. *arXiv preprint arXiv:1406.3385* 2014.
(47) Sanjines, R.; Tang, H.; Berger, H.; Gozzo, F.; Margaritondo, G.; Levy, F. Electronic structure of anatase TiO_2 oxide. *J. Appl. Phys.* **1994**, *75*, 2945–2951.
(48) Qiu, J.; Zeng, G.; Ha, M.; Hou, B.; Mecklenburg, M.; Shi, H.; Alexandrova, A. N.; Cronin, S. B. A Microscopic Study of Atomic Layer Deposition of TiO_2 on GaAs and its Photocatalytic Application. *Chem. Mater.* **2015**, *27*, 7977–7981.
(49) Qiu, J.; Zeng, G.; Ha, M.; Ge, M.; Lin, Y.; Hettick, M.; Hou, B.; Alexandrova, A. N.; Javey, A.; Cronin, S. B. Artificial Photosynthesis on TiO_2-Passivated InP Nanopillars. *Nano Lett.* **2015**, *15*, 6177–6181.

DOI: 10.1021/acs.jctc.6b00095
J. Chem. Theory Comput. XXXX, XXX, XXX–XXX